

Neutron-skin values and matter and neutron radii determined from reaction cross sections of proton scattering on ^{12}C , $^{40,48}\text{Ca}$, ^{58}Ni , ^{208}Pb

Tomotsugu Wakasa

Department of Physics, Kyushu University, Fukuoka 819-0395, Japan

Shingo Tagami

Department of Physics, Kyushu University, Fukuoka 819-0395, Japan

Jun Matsui

Department of Physics, Kyushu University, Fukuoka 819-0395, Japan

Maya Takechi

Niigata University, Niigata 950-2181, Japan

Masanobu Yahiro*

Department of Physics, Kyushu University, Fukuoka 819-0395, Japan

(Dated: December 29, 2022)

Background: Very lately, the PREX and the CREX collaboration present skin values, $r_{\text{skin}}^{208}(\text{newPREX2}) = 0.278 \pm 0.078$ (exp) ± 0.012 (theor.) fm and $r_{\text{skin}}^{48} = 0.121 \pm 0.026$ (exp) ± 0.024 (model), respectively. We recently determined a neutron-skin value $r_{\text{skin}}^{208} = 0.278 \pm 0.035$ fm from measured reaction cross sections $\sigma_{\text{R}}(\text{exp})$ of $\text{p}+^{208}\text{Pb}$ scattering in a range of incident energies $10 \leq E_{\text{in}} \leq 100$ MeV where the chiral (Kyushu) g -matrix folding model is reliable for $^{12}\text{C}+^{12}\text{C}$ scattering. The data $\sigma_{\text{R}}(\text{exp})$ are available for proton scattering on ^{58}Ni , $^{40,48}\text{Ca}$, ^{12}C targets.

Purpose: Our first aim is to test the Kyushu g -matrix folding model for $\text{p}+^{208}\text{Pb}$ scattering in $20 \leq E_{\text{in}} \leq 180$ MeV. Our second aim is to determine skin values r_{skin} and matter and neutron radii, r_{m} and r_{n} , for ^{208}Pb , ^{58}Ni , $^{40,48}\text{Ca}$, ^{12}C from the $\sigma_{\text{R}}(\text{exp})$.

Methods: Our method is the Kyushu g -matrix folding model with the densities scaled from the DIS-GHFB+AMP densities, where DIS-GHFB+AMP stands for Gogny-DIS HFB (GHFB) with the angular momentum projection (AMP).

Results: As for proton scattering, we find that our model is reliable in $20 \leq E_{\text{in}} \leq 180$ MeV. For ^{208}Pb , the skin value deduced from $\sigma_{\text{R}}(\text{exp})$ in $20 \leq E_{\text{in}} \leq 180$ MeV is $r_{\text{skin}}^{208}(\sigma_{\text{R}}) = 0.299 \pm 0.020$ fm. Our results on r_{skin} are compared with the previous works.

Conclusion: Our result $r_{\text{skin}}^{208}(\sigma_{\text{R}}) = 0.299 \pm 0.020$ fm agrees with $r_{\text{skin}}^{208}(\text{PREX2}) = 0.283 \pm 0.071$ fm. In addition, our result $r_{\text{skin}}^{48} = 0.103 \pm 0.022$ fm is consistent with the CREX value.

I. INTRODUCTION

Many theoretical predictions on the symmetry energy $S_{\text{sym}}(\rho)$ have been made so far by taking several experimental and observational constraints on $S_{\text{sym}}(\rho)$ and their combinations. In neutron star (NS), the $S_{\text{sym}}(\rho)$ and its density (ρ) dependence influence strongly the nature within the star. The symmetry energy $S_{\text{sym}}(\rho)$ cannot be measured by experiment directly. In place of $S_{\text{sym}}(\rho)$, the neutron-skin thickness r_{skin} is measured to determine the slope parameter L , since a strong correlation between r_{skin}^{208} and L is well known [1].

Horowitz *et al.* [2] proposed a direct measurement for neutron skin thickness $r_{\text{skin}} = r_{\text{n}} - r_{\text{p}}$, where r_{n} and r_{p} are the root-mean-square radii of neutrons and protons, respectively.

The PREX collaboration has reported a new value,

$$r_{\text{skin}}^{208}(\text{PREX2}) = 0.283 \pm 0.071 \text{ fm}, \quad (1)$$

combining the original Lead Radius EXperiment (PREX) result [3, 4] with the updated PREX2 result [5]. Very lately, the

PREX collaboration has presented an accurate value[?],

$$r_{\text{skin}}^{208}(\text{newPREX2}) = 0.278 \pm 0.078 \text{ (exp)} \pm 0.012 \text{ (theor.) fm}, \quad (2)$$

The value is most reliable for ^{208}Pb . The $r_{\text{skin}}^{208}(\text{PREX2})$ value is considerably larger than the other experimental values that are significantly model dependent [6–9]. As an exceptional case, a nonlocal dispersive-optical-model (DOM) analysis of ^{208}Pb deduces $r_{\text{skin}}^{\text{DOM}} = 0.25 \pm 0.05$ fm [10] consistent with $r_{\text{skin}}^{208}(\text{PREX2})$.

Very recently, the CREX group has presented [11]

$$r_{\text{skin}}^{48}(\text{CREX}) = 0.121 \pm 0.026 \text{ (exp)} \pm 0.024 \text{ (model) fit}(\text{fit})$$

The CREX value is most reliable for ^{48}Ca .

The $r_{\text{skin}}^{208}(\text{PREX2})$ provides crucial tests for the equation of state (EoS) of nuclear matter [12–16]. For example, Reed *et al.* [17] report a value of the slope parameter L and examine the impact of such a stiff symmetry energy on some critical NS observables. They deduce

$$L = 106 \pm 37 = 69\text{--}143 \text{ MeV} \quad (4)$$

from $r_{\text{skin}}^{208}(\text{PREX2})$.

In Ref. [18], we accumulated the 206 EoSs from Refs. [1, 19–43] in which r_{skin}^{208} and/or L is presented. The correlation

* orion093g@gmail.com

between r_{skin}^{208} and L is more reliable when the number of EoSs is larger. The resulting relation

$$L = 620.39 r_{\text{skin}}^{208} - 57.963 \text{ MeV} \quad (5)$$

has a strong correlation with the correlation coefficient $R = 0.99$, as shown in Fig. 1.

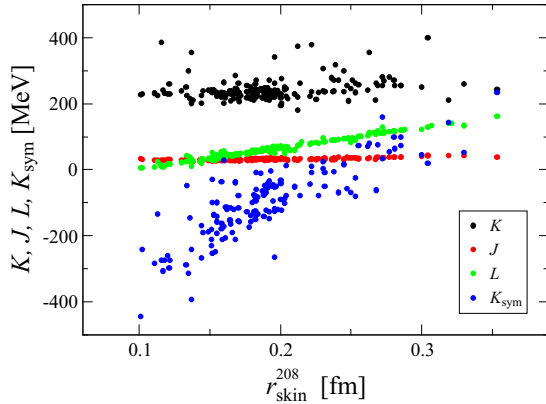


FIG. 1. r_{skin}^{208} dependence of J , L , K_{sym} , where J , L , K_{sym} are a constant term, the first-derivative and the second-derivative term of the symmetry energy. The dots show 206 EoSs taken from Table of Ref. [18]. Obviously, the correlation between r_{skin}^{208} and L is linear.

The relation (5) allows us to deduce a constraint on L from the PREX2 value. The resulting range of L are $L = 76\text{--}165$ MeV, while equation shown in Ref. [1] yields $L = 76\text{--}172$ MeV. These values and $L = 69\text{--}143$ MeV support stiffer EoSs. The stiffer EoSs allow us to consider the phase transition such as QCD transition in NS. The following EoSs satisfy $L = 76\text{--}172$ MeV; SkO, FKVW, Rs, SV-sym34, es325, TFa, NL ρ , BSR6, R σ , Sk-Rs, E0009, Gs, Z271, GM3, PKDD, E0008(TMA), SK272, GM1, G σ , Sk-T4, SK255, SV, es35, S271, SkI3, rG2, PC-PK1, SkI2, E0025, PC-LA, rNLC, E0036, rTM1, TM1, NL4, rNL-SH, NL-SH, rNL-RA1, PC-F2, PK1, PC-F1, NL3, rNL3, PC-F3, PC-F4, NL3*, TFb, rNL3*, SkI5, NL2, rNL-Z, TFC, NL1, rNL1, SkI1 in Table I of Ref. [18].

As an indirect measurement, meanwhile, the high-resolution $E1$ polarizability experiment ($E1pE$) yields

$$r_{\text{skin}}^{208}(E1pE) = 0.156_{-0.021}^{+0.025} = 0.135\text{--}0.181 \text{ fm} \quad (6)$$

for ^{208}Pb [44]

$$r_{\text{skin}}^{48}(E1pE) = 0.17 \pm 0.03 = 0.14\text{--}0.20 \text{ fm} \quad (7)$$

for ^{48}Ca [45].

There is no overlap between $r_{\text{skin}}^{208}(\text{PREX2})$ and $r_{\text{skin}}^{208}(E1pE)$ in one σ level. However, we determined a value of $r_{\text{skin}}^{208}(\text{exp})$ from measured reaction cross sections $\sigma_{\text{R}}(\text{exp})$ of $\text{p}+^{208}\text{Pb}$ scattering in a range of incident energies, $30 \lesssim E_{\text{in}} \lesssim 100$ MeV [46]; the

value is $r_{\text{skin}}^{208}(\text{exp}) = 0.278 \pm 0.035$ fm. Our result agrees with $R_{\text{skin}}^{208}(\text{PREX2})$. We also deduced $r_{\text{n}}(\text{exp}) = 5.722 \pm 0.035$ fm and $r_{\text{m}}(\text{exp}) = 5.614 \pm 0.022$ fm in addition to $r_{\text{skin}}^{208}(\text{exp})$. As for $\text{He}+^{208}\text{Pb}$ scattering, we determine $r_{\text{skin}}^{208}(\text{exp}) = 0.416 \pm 0.146$ fm [47]. Our results are consistent with PREX II and therefore supports larger slope parameter L .

Our model is the chiral (Kyushu) g -matrix folding model with the densities calculated with Gogny-D1S HFB (D1S-GHFB) with the angular momentum projection (AMP) [48, 49]. For $\text{p}+^{208}\text{Pb}$ scattering, the neutron density is scaled so that the r_{n} of the scaled neutron density can reproduce the data [50–52] on σ_{R} , since the r_{p} of D1S-GHFB+AMP proton density agrees with the $r_{\text{p}}(\text{exp})$ [53] determined from electron scattering. For ^{12}C scattering on ^9Be , ^{12}C , ^{27}Al targets, we tested reliability of the Kyushu g -matrix folding model and found that the Kyushu g -matrix folding model is reliable in $30 \lesssim E_{\text{in}} \lesssim 100$ MeV and $250 \lesssim E_{\text{in}} \lesssim 400$ MeV [49]. This is the reason why we took $30 \lesssim E_{\text{in}} \lesssim 100$ MeV in the analyses [46] of $\text{p}+^{208}\text{Pb}$ scattering. After the analyses, we find that the Kyushu g -matrix folding model reproduces the lower bound of the data on σ_{R} [54] for $^{12}\text{C}+^{12}\text{C}$ scattering at $E_{\text{in}} = 10.4$ MeV per nucleon.

The g -matrix folding model is a standard way of deriving the microscopic optical potential for proton scattering and nucleus-nucleus scattering [49, 55–64]. The folding model is composed of the single folding model for proton scattering and the double folding model for nucleus-nucleus scattering. The relation between the single and the double folding model is clearly shown in Ref. [60]. Applying the double-folding model based on Melbourne g -matrix [58] for the data [65] on interaction cross sections, we found that ^{31}Ne is a halo nucleus with large deformation [64], and deduced the matter radii r_{m} for Ne isotopes [66]. Also for Mg isotopes, we determined the r_{m} from $\sigma_{\text{R}}(\text{exp})$ for scattering of Mg isotopes on a ^{12}C target [67].

Now, we consider proton scattering on ^{208}Pb , ^{58}Ni , $^{40,48}\text{Ca}$, ^{12}C targets, since there is no interaction cross section for proton scattering. In fact, good data on σ_{R} are available in Refs. [50–52] for ^{208}Pb , Refs [51, 52, 68–70] for ^{58}Ni , Ref. [71] for ^{48}Ca , Refs. [50–52] for ^{40}Ca , and Refs. [51, 52, 72] for ^{12}C . We have already shown that for $\text{p}+^{208}\text{Pb}$ scattering the σ_{R} calculated with $r_{\text{skin}}^{208}(\text{PREX2})$ and $r_{\text{p}}(\text{exp}) = 5.444$ fm [53] of electron scattering reproduce the data at $E_{\text{lab}} = 534.1, 549, 806$ MeV [73].

In this paper, we first test the Kyushu g -matrix single folding model for $\text{p}+^{208}\text{Pb}$ scattering, since the PREX2 data is available. We find that the present model is reliable in $20 \lesssim E_{\text{in}} \lesssim 180$ MeV, as shown in Sec. III A. After the testing, we determine $r_{\text{m}}(\text{exp})$, $r_{\text{n}}(\text{exp})$, $r_{\text{skin}}(\text{exp})$ for ^{208}Pb , ^{58}Ni , $^{40,48}\text{Ca}$, ^{12}C from the $\sigma_{\text{R}}(\text{exp})$ in $20 \lesssim E_{\text{in}} \lesssim 180$ MeV, as shown in Sec. III B. For each nucleus, the D1S-GHFB+AMP proton and neutron densities are scaled so as to reproduce $\sigma_{\text{R}}(\text{exp})$ under that condition that the $r_{\text{p}}(\text{scaling})$ of the scaled proton density agrees with $r_{\text{p}}(\text{exp})$ of electron scattering.

We explain our model in Sec. II and our results in Sec. III. Section IV is devoted to a summary.

II. MODEL

Our model is the Kyushu g -matrix folding model [48, 49] with the proton and neutron densities scaled from the D1S-GHFB+AMP densities.

A. The Kyushu g -matrix folding model

Kohno calculated the g matrix for the symmetric nuclear matter, using the Brueckner-Hartree-Fock method with chiral N^3 LO 2NFs and NNLO 3NFs [74], where N^3 LO 3NF is abbreviation of next-to-next-to-next-to-leading-order three-body force and NNLO 2NFs is of next-to-next-to-leading-order two-body force. He set $c_D = -2.5$ and $c_E = 0.25$ so that the energy per nucleon can become minimum at $\rho = \rho_0$; see Fig. 2 for the definition of c_D and c_E . Toyokawa *et al.* localized the non-local chiral g matrix into three-range Gaussian forms [48], using the localization method proposed by the Melbourne group [58, 75, 76]. The resulting local g matrix is referred to as ‘‘Kyushu g -matrix’’. The Kyushu g -matrix is constructed from chiral interaction with the cutoff 550 MeV. fig-chiral.epsfig-chiral

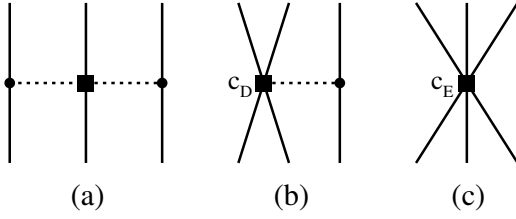


FIG. 2. 3NFs in NNLO (next-to-next-to-leading-order). Diagram (a) corresponds to the Fujita-Miyazawa 2π -exchange 3NF (next-to-next-to-next-to-leading-order) [77], and diagrams (b) and (c) correspond to 1π -exchange and contact 3NFs. The solid and dashed lines denote nucleon and pion propagations, respectively, and filled circles and squares stand for vertices. The strength of the filled-square vertex is often called c_D in diagram (b) and c_E in diagram (c).

The Kyushu g -matrix folding model is successful in reproducing σ_R , differential cross sections $d\sigma/d\Omega$, vector analyzing powers A_y for ^4He scattering in $E_{\text{in}} = 30\text{--}200$ MeV per nucleon [48]. The success is true for proton scattering at $E_{\text{in}} = 65$ MeV [78].

In Ref. [79], we tested the Kyushu g -matrix folding model [48] for ^{12}C scattering on ^9Be , ^{12}C , ^{27}Al targets in $30 \leq E_{\text{in}} \leq 400$ MeV. We found that the Kyushu g -matrix folding model is reliable for σ_R in $30 \leq E_{\text{in}} \leq 100$ MeV and $250 \leq E_{\text{in}} \leq 400$ MeV. This indicates that the Kyushu g -matrix folding model is applicable in the E_{in} range. After the test, we found that our model reproduces the lower bound of measured reaction cross section σ_R [54] at $E_{\text{in}} = 10.4$ MeV. Our model is reliable for $10 \leq E_{\text{in}} \leq 100$ MeV and $250 \leq E_{\text{in}} \leq 400$ MeV.

We recapitulate the single folding model for nucleon-nucleus scattering. The potential $U(\mathbf{R})$ consists of the direct

and exchange parts [60], $U^{\text{DR}}(\mathbf{R})$ and $U^{\text{EX}}(\mathbf{R})$, defined by

$$U^{\text{DR}}(\mathbf{R}) = \sum_{\mu,\nu} \int \rho_T^\nu(\mathbf{r}_T) g_{\mu\nu}^{\text{DR}}(s; \rho_{\mu\nu}) d\mathbf{r}_T, \quad (8a)$$

$$U^{\text{EX}}(\mathbf{R}) = \sum_{\mu,\nu} \int \rho_T^\nu(\mathbf{r}_T, \mathbf{r}_T + \mathbf{s}) \times g_{\mu\nu}^{\text{EX}}(s; \rho_{\mu\nu}) \exp[-i\mathbf{K}(\mathbf{R}) \cdot \mathbf{s}/M] d\mathbf{r}_T \quad (8b)$$

where \mathbf{R} is the relative coordinate between a projectile (P) and a target (T), $\mathbf{s} = -\mathbf{r}_T + \mathbf{R}$, and \mathbf{r}_T is the coordinate of the interacting nucleon from the center-of-mass of T. Each of μ and ν denotes the z -component of isospin, i.e., $(1/2, -1/2)$ corresponds to (neutron, proton). The nonlocal U^{EX} has been localized in Eq. (8b) with the local semi-classical approximation [55], where $\mathbf{K}(\mathbf{R})$ is the local momentum between P and T, and $M = A/(1+A)$ for the target mass number A ; see Ref. [80] for the validity of the localization. The direct and exchange parts, $g_{\mu\nu}^{\text{DR}}$ and $g_{\mu\nu}^{\text{EX}}$, of the g -matrix depend on the local density

$$\rho_{\mu\nu} = \sigma^\mu \rho_T^\nu(\mathbf{r}_T + \mathbf{s}/2) \quad (9)$$

at the midpoint of the interacting nucleon pair, where σ^μ having $\mu = -1/2$ is the Pauli matrix of an incident proton. As a way of taking the center-of-mass correction to the D1S-GHFB+AMP densities, we use the method of Ref. [66], since the procedure is quite simple.

The direct and exchange parts, $g_{\mu\nu}^{\text{DR}}$ and $g_{\mu\nu}^{\text{EX}}$, of the g -matrix, are described by [66]

$$\begin{aligned} & g_{\mu\nu}^{\text{DR}}(s; \rho_{\mu\nu}) \\ &= \begin{cases} \frac{1}{4} \sum_S \hat{S}^2 g_{\mu\nu}^{S1}(s; \rho_{\mu\nu}) & ; \text{ for } \mu + \nu = \pm 1 \\ \frac{1}{8} \sum_{S,T} \hat{S}^2 g_{\mu\nu}^{ST}(s; \rho_{\mu\nu}), & ; \text{ for } \mu + \nu = 0 \end{cases} \quad (10) \\ & g_{\mu\nu}^{\text{EX}}(s; \rho_{\mu\nu}) \\ &= \begin{cases} \frac{1}{4} \sum_S (-1)^{S+1} \hat{S}^2 g_{\mu\nu}^{S1}(s; \rho_{\mu\nu}) & ; \text{ for } \mu + \nu = \pm 1 \\ \frac{1}{8} \sum_{S,T} (-1)^{S+T} \hat{S}^2 g_{\mu\nu}^{ST}(s; \rho_{\mu\nu}) & ; \text{ for } \mu + \nu = 0 \end{cases} \quad (11) \end{aligned}$$

where $\hat{S} = \sqrt{2S+1}$ and $g_{\mu\nu}^{ST}$ are the spin-isospin components of the g -matrix; see Ref. [63] for the explicit form of $g_{\mu\nu}^{\text{DR}}$ and $g_{\mu\nu}^{\text{EX}}$.

The potential $U(\mathbf{R})$ thus obtained has the form of $U(\mathbf{R}) = U_{\text{cent}}(R) + \hat{\ell} \cdot \hat{\sigma} U_{\text{spin-orbit}}(R)$, where $U_{\text{cent}}(R)$ and $U_{\text{spin-orbit}}(R)$ are the central and the spin-orbit part of $U(\mathbf{R})$, respectively, and ℓ is the orbital angular momentum of the proton scattering; see Eq. (28) in Ref. [81] for the derivation. The relative wave function ψ between P and T can be decomposed into partial waves χ_ℓ , each with different ℓ . The χ_ℓ is obtained by solving the Schrödinger equation having $U(\mathbf{R})$. The elastic S -matrix elements S_ℓ are obtained from the asymptotic

form of χ_ℓ . The total reaction cross section σ_R is calculable from the S_ℓ as

$$\sigma_R = \frac{\pi}{K^2} \sum_\ell (2\ell + 1)(1 - |S_\ell|^2). \quad (12)$$

B. Scaling procedure of proton and neutron densities

The proton and neutron densities, $\rho_p(r)$ and $\rho_n(r)$, are scaled from the D1S-GHFB+AMP densities. We can obtain the scaled density $\rho_{\text{scaling}}(\mathbf{r})$ from the original density $\rho(\mathbf{r})$ as

$$\rho_{\text{scaling}}(\mathbf{r}) = \frac{1}{\alpha^3} \rho(\mathbf{r}/\alpha) \quad (13)$$

with a scaling factor

$$\alpha = \sqrt{\frac{\langle r^2 \rangle_{\text{scaling}}}{\langle r^2 \rangle}}. \quad (14)$$

For later convenience, we refer to the proton (neutron) radius of the scaled proton (neutron) density $\rho_{\text{scaling}}^p(\mathbf{r})$ ($\rho_{\text{scaling}}^n(\mathbf{r})$) as $r_p(\text{scaling})$ ($r_n(\text{scaling})$).

Table IV shows the scaling factors, α_p and α_n , from the D1S-GHFB+AMP densities to the scaled densities that reproduce data $\sigma_R(\text{exp})$ and $r_p(\text{exp})$ of electron scattering.

TABLE I. Scaling factors α_n and α_p for neutron and proton.

	α_n	α_p
^{208}Pb	1.015	1.000
^{58}Ni	1.003	0.994
^{48}Ca	0.973	0.982
^{40}Ca	1.000	0.995
^{12}C	0.942	0.957

C. Effective nucleon-nucleon interaction for targets

For a change of the proton and neutron distributions in targets, a microscopic approach is to modify D1S. For the Gogny EoSs, the effective nucleon-nucleon interaction can be described as

$$\begin{aligned} V(\vec{r}) = & \sum_{i=1,2} t_0^i (1 + x_0^i P_\sigma) \rho^{\alpha_i} \delta(\vec{r}) \\ & + \sum_{i=1,2} (W_i + B_i P_\sigma - H_i P_\tau - M_i P_\sigma P_\tau) e^{-\frac{r^2}{\mu_i^2}} \\ & + iW_0(\sigma_1 + \sigma_2)[\vec{k}^j \times \delta(\vec{r})\vec{k}], \end{aligned} \quad (15)$$

where σ and τ are the Pauli spin and isospin operators, respectively, and the corresponding exchange operators P_σ and P_τ are defined as usual.

For ^{208}Pb , we have changed all parameters of D1S, but cannot find the NN interaction that reproduce $r_{\text{skin}}^{208}(\text{PREX2}) =$

0.283 ± 0.071 fm. The best fitting is the D1PK2-GHFB+AMP with $r_{\text{skin}}^{208}(\text{D1PK2}) = 0.185$ fm; note that $r_{\text{skin}}^{208}(\text{D1S}) = 0.137$ fm. The parameters of D1PK2 are shown in Table II.

TABLE II. Parameter sets of D1PK2.

D1PK	μ_i	W_i	B_i	H_i	M_i	t_0^i	x_0^i	α_i	W_0
$i = 1$	0.90	-465.027582	155.134492	-506.775323	117.749903	981.065351	1	1/3	130
$i = 2$	1.44	34.6200000	-14.0800000	70.9500000	-41.3518104	534.155654	-1	1	

III. RESULTS

First of all, we regard reliable r_m and r_n as reference values, $r_m(\text{ref})$ and $r_n(\text{ref})$, in order to determine $r_m(\text{exp})$ from $\sigma_R(\text{exp})$. The reference values are shown below; see Table III for the numerical values. Whenever we calculate σ_R , we use the Kyushu g -matrix model.

^{58}Ni : The reference values are the $r_m(\text{AMP})$ and $r_n(\text{AMP})$ calculated with D1S-GHFB+AMP, since the $\sigma_R(\text{AMP})$ are near the upper bound of the data, as shown in Fig. 5. E_{in} dependence of $\sigma_R(\text{AMP})$ is similar to that of the data. We then define the ratio $F(E_{\text{in}}) \equiv \sigma_R(\text{exp})/\sigma_R(\text{ref}) = \sigma_R(\text{exp})/\sigma_R(\text{AMP})$, and introduce the average value of $F(E_{\text{in}})$ as a fine-tuning factor F . The factor is $F = 0.96473$ close to 1. The $F\sigma_R(\text{AMP})$ almost reproduce the central values of the data, as shown in Fig. 5. The scaling procedure is not made to get the reference values, i.e., $\alpha = 1$.

^{208}Pb : The reference values are the $r_m(\text{PREX2})$ and $r_n(\text{PREX2})$ evaluated from $r_{\text{skin}}^{208}(\text{PREX2})$ and $r_p(\text{exp})$ [53] of electron scattering. In this case, the $\sigma_R(\text{exp})$ based on the densities scaled to $r_n(\text{PREX2})$ and $r_p(\text{exp})$ reproduce the data within error-bar, as shown in Fig. 3. For this reason, F is 1.

^{48}Ca : We can obtain $r_m(\text{CREX})$ and $r_n(\text{CREX})$ from the CREX value of Eq. (3) and $r_p(\text{exp}) = 3.385$ fm [82] of electron scattering. In this case, the $\sigma_R(\text{CREX})$ based on $r_n(\text{CREX})$ and $r_p(\text{exp})$ are near the central values of the data, as shown in Fig. 6. The fine-tuning factor is $F = 0.9810$ close to 1. The $F\sigma_R(E1pE)$ almost reproduce the central values of the data, as shown in Fig. 6.

^{40}Ca : As for $^{40,48}\text{Ca}$, Zenihiro *et al.* measured the differential cross section and the analyzing powers for $p+^{40,48}\text{Ca}$ scattering in RCNP, and determined $r_{\text{skin}}^{40,48}(\text{RCNP})$ [83]. For ^{48}Ca , the value $r_{\text{skin}}(\text{RCNP}) = 0.168_{-0.028}^{+0.025}$ fm is consistent with $r_{\text{skin}}^{48}(E1pE)$. For ^{40}Ca , their values are shown in Table III as reference values. Since $\sigma_R(\text{RCNP}) = \sigma_R(\text{AMP})$, the $\sigma_R(\text{AMP})$ are reliable. In this case, the $\sigma_R(\text{AMP})$ overshoot the data, as shown in Fig. 7. The fine-tuning factor is $F = 0.92716$ close to 1. The $F\sigma_R(\text{AMP})$ almost reproduce the central values of the data, as shown in Fig. 7.

^{12}C : Tanihata *et al.* measured interaction cross sections at 790 MeV/nucleon in GSI and determined $r_m(\text{GSI}) = 2.35$ fm for ^{12}C [84]. The $r_m(\text{GSI})$ and $r_p(\text{exp}) = 2.327$ fm [82] lead to $r_n(\text{GSI}) = 2.37$ fm. The $r_m(\text{GSI})$ and $r_n(\text{GSI})$ are reference values. The fine-tuning factor is $F = 0.93077$ close to 1. The $F\sigma_R(\text{GSI})$ are near the central values of $\sigma_R(\text{exp})$, as shown in Fig. 8.

TABLE III. Reference values of $r_m(\text{ref})$, $r_n(\text{ref})$, $r_{\text{skin}}(\text{ref})$ together with $r_p(\text{exp})$ of electron scattering. The $r_p(\text{exp})$ are deduced from the electron scattering [53, 82]. In actual calculations, the central values are taken as reference values. The radii are shown in units of fm.

	Ref.	$r_p(\text{exp})$	$r_m(\text{ref})$	$r_n(\text{ref})$	$r_{\text{skin}}(\text{ref})$
^{208}Pb	PREX2	5.444	5.617 ± 0.044	5.727 ± 0.071	0.283 ± 0.071
^{58}Ni	D1S AMP	3.727	3.721	3.715	-0.013
^{48}Ca	CREX	3.385	3.456 ± 0.050	3.506 ± 0.050	0.121 ± 0.050
^{40}Ca	[83]	3.385	$3.380^{+0.022}_{-0.023}$	$3.375^{+0.022}_{-0.023}$	$-0.010^{+0.022}_{-0.023}$
^{12}C	[84]	2.327	2.35 ± 0.02	2.37 ± 0.02	0.05 ± 0.02

TABLE IV. Fine-tuning factor F .

	F
^{208}Pb	1
^{58}Ni	0.96473
^{48}Ca	0.9810
^{40}Ca	0.92716
^{12}C	0.93077

When we determine $r_m(\text{exp})$ from data $\sigma_R(\text{exp})$, we scale the D1S-GHFB+AMP proton and neutron densities so as to $F\sigma_R(\text{ref}) = \sigma_R(\text{exp})$ and $r_p(\text{scaling}) = r_p(\text{exp})$. Next, we deduce $r_m(\text{exp})$ from $r_n(\text{scaling})$ and $r_p(\text{scaling})$ for each E_{in} . The resulting $r_m(\text{exp})$ depends on E_{in} . For all the $r_m(\text{exp})$, we take the weighted mean and its error. Finally, we evaluate $r_{\text{skin}}(\text{exp})$ and $r_n(\text{exp})$ from the resulting $r_m(\text{exp})$ and the $r_p(\text{exp})$ [53, 82] of the electron scattering. For later convenience, we refer to this procedure as “experimental scaling procedure with F (ESP-F)”.

A. Test of the Kyushu g -matrix folding model for $p+^{208}\text{Pb}$ scattering

Now we test the Kyushu g -matrix model for proton scattering. As shown in Fig. 3, the σ_R (squares with error bar) based on R_{skin}^{208} (PREX2) and $r_p(\text{exp})$ are consistent with data [50–52] in $20 \leq E_{\text{in}} \leq 180$ MeV; see Table III for R_{skin}^{208} (PREX2) and $r_p(\text{exp})$. This indicates that our model is good in $20 \leq E_{\text{in}} \leq 180$ MeV for proton scattering.

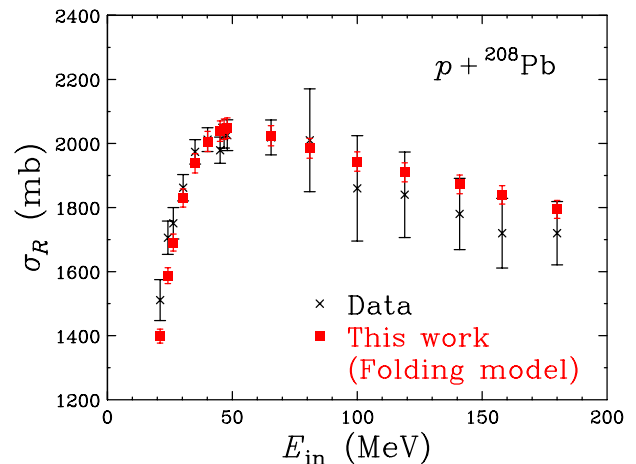


FIG. 3. E_{in} dependence of reaction cross sections σ_R for $p+^{208}\text{Pb}$ scattering. The squares with error bar (legend “This work (Folding model)”) stand for the results of the folding model with the densities scaled to PREX2, whereas the crosses with error bar correspond to the data [50–52] on σ_R .

B. ^{208}Pb , ^{58}Ni , $^{48,40}\text{Ca}$, ^{12}C

1. ^{208}Pb

Figure 4 shows reaction cross sections σ_R of $p+^{208}\text{Pb}$ scattering as a function of E_{in} . The results of the D1S-GHFB+AMP densities reproduce the data [50–52] with 4% errors. This is true for the neutron density scaled to the central value of PREX2 and the D1S-GHFB+AMP density. In the results of the Woods-Saxon type neutron density ($r_{WS} = 6.59$ fm, $a_{WS} = 0.7$ fm) fitted to the central value of PREX2, we use the D1S-GHFB+AMP proton density. The results of the Woods-Saxon type neutron density ($r_{WS} = 6.59$ fm, $a_{WS} = 0.7$ fm) and the D1S-GHFB+AMP proton density are close to those of the neutron density scaled to the central value of PREX2 and the D1S-GHFB+AMP proton density. The Woods-Saxon type neutron density ($r_{WS} = 6.81$ fm, $a_{WS} = 0.6$ fm) yields almost the same results as the case of $r_{WS} = 6.59$ fm, $a_{WS} = 0.7$ fm, that is, the former under-shoots the latter by 0.974. We then do not show the former results in Fig. 4.

The results of ESP-F are $r_{\text{skin}}^{208}(\text{exp}) = 0.299 \pm 0.020$ fm, $r_n(\text{exp}) = 5.743 \pm 0.020$ fm, $r_m(\text{exp}) = 5.627 \pm 0.020$ fm. The present skin value 0.299 ± 0.020 fm almost agrees with our previous value $r_{\text{skin}}^{208}(\text{exp}) = 0.278 \pm 0.035$ fm of Ref. [46].

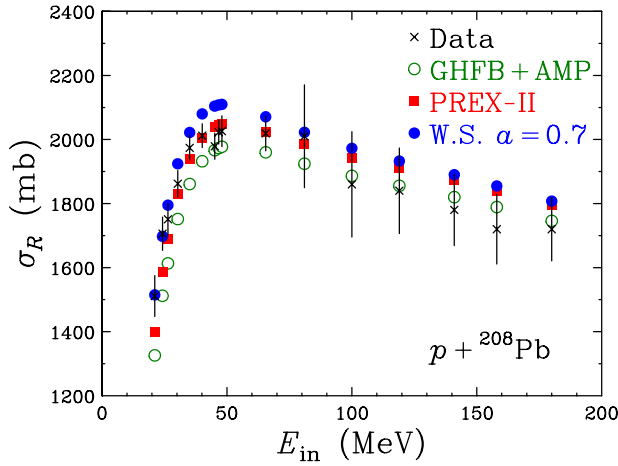


FIG. 4. E_{in} dependence of reaction cross sections σ_R for $p+^{208}\text{Pb}$ scattering. Squares stand for the results of the folding model with the neutron density scaled to the central value of PREX2. Open circles denote the results of the D1S-GHFB+AMP densities, and close circles correspond to the results of the Woods-Saxon type neutron density ($r_{WS} = 6.59$ fm, $a_{WS} = 0.7$ fm) fitted to the central value of PREX2. As for the proton density, it is calculated with D1S-GHFB+AMP for three types of calculations. The crosses with error bar are the data [50–52] on σ_R .

2. ^{58}Ni

Figure 5 shows σ_R as a function of E_{in} for $p+^{58}\text{Ni}$ scattering. The results $\sigma_R(\text{AMP})$ of the Kyushu g -matrix folding model with the D1S-GHFB+AMP densities (closed circles) almost reproduces data $\sigma_R(\text{exp})$ [51, 52, 68–70] in $10 \lesssim E_{\text{in}} \lesssim 81$ MeV; note that the data has high accuracy of 2.7%.

The result of ESP-F is $r_m(\text{exp}) = 3.711 \pm 0.010$ fm. Using the $r_m(\text{exp})$ and $r_p(\text{exp}) = 3.685$ fm [82], we can obtain $r_{\text{skin}} = 0.055 \pm 0.010$ fm and $r_n = 3.740 \pm 0.010$ fm.

A novel method for measuring nuclear reactions in inverse kinematics with stored ion beams was successfully used to extract the matter radius of ^{58}Ni [85]. The experiment was performed at the experimental heavy-ion storage ring at the GSI facility. Their results determined from the differential cross section for $^{58}\text{Ni}+^4\text{He}$ scattering are $r_m(\text{GSI}) = 3.70(7)$ fm, $r_p(\text{GSI}) = 3.68$ fm, $r_n(\text{GSI}) = 3.71(12)$ fm, $r_{\text{skin}}(\text{GSI}) = 0.03(12)$ fm.

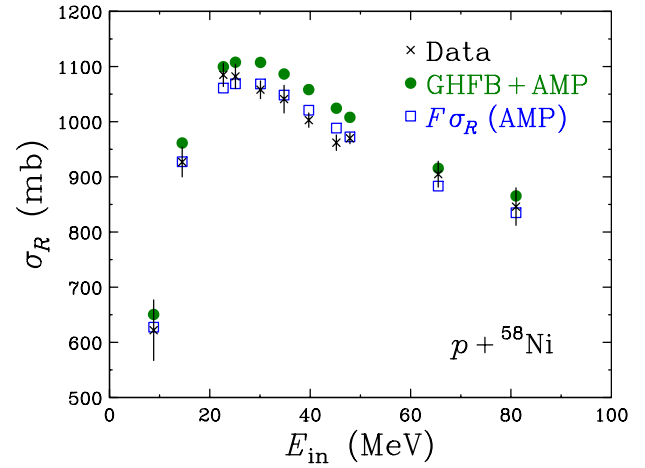


FIG. 5. E_{in} dependence of reaction cross sections σ_R for $p+^{58}\text{Ni}$ scattering. Closed circles denote results of the D1S-GHFB+AMP densities. Squares stand for $F\sigma_R(\text{AMP})$ with $F = 0.96473$. The data (crosses) are taken from Refs. [51, 52, 68–70].

3. ^{48}Ca

Figure 6 shows σ_R as a function of E_{in} for $p+^{48}\text{Ca}$ scattering. The $\sigma_R(\text{AMP})$ almost reproduce the data [71]. The results $\sigma_R(\text{CREX})$ based on $r_n(\text{CREX})$ and $r_p(\text{exp})$ [82] are near the central values of the data [71]. E_{in} dependence of $\sigma_R(E1pE)$ is similar to that of the data [71]. The $F\sigma_R(\text{CREX})$ almost reproduce the central values of the data.

The results of ESP-F are $r_{\text{skin}} = 0.103 \pm 0.022$ fm and $r_n = 3.488 \pm 0.022$ fm. Our skin value agrees with $r_{\text{skin}}^{48}(\text{CREX})$.

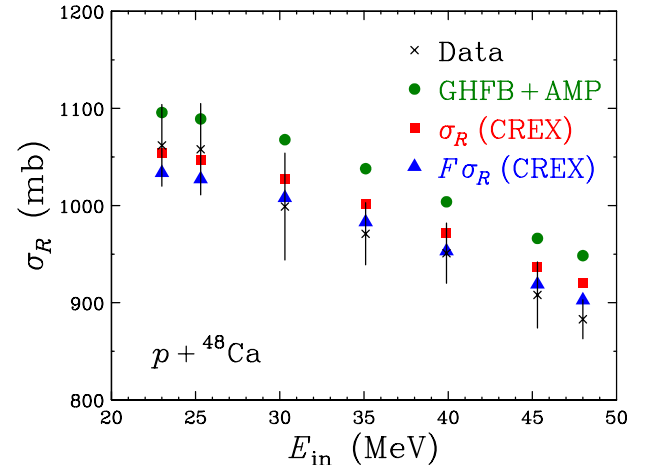


FIG. 6. E_{in} dependence of reaction cross sections σ_R for $p+^{48}\text{Ca}$ scattering. Circles denote results of the D1S-GHFB+AMP densities, and squares correspond to the results of the scaled densities based on $r_{\text{skin}}^{48}(\text{CREX})$. Triangles stand for $F\sigma_R(\text{CREX})$ with $F = 0.9810$. The data (crosses) are taken from Ref. [71].

4. ^{40}Ca

Figure 7 shows σ_R as a function of E_{in} for $p+^{40}\text{Ca}$ scattering. The Kyushu g -matrix folding model with the D1S-GHFB+AMP densities overestimates $\sigma_R(\text{exp})$ [50–52]; note that the data has high accuracy of 2.7 %. Note that $\sigma_R(\text{AMP}) = \sigma_R(\text{PCNP})$, since $r_m(\text{AMP})$ is very close to $r_m(\text{RCNP})$. E_{in} dependence of $\sigma_R(\text{AMP})$ is similar to that of the data [50–52].

The result of ESP-F is $r_m(\text{exp}) = 3.372 \pm 0.011$ fm. Using the $r_m(\text{exp})$ and $r_p(\text{exp}) = 3.378$ fm of electron scattering, we can obtain $r_{\text{skin}}(\text{exp}) = -0.011 \pm 0.011$ fm and $r_n(\text{exp}) = 3.367 \pm 0.011$ fm. Our results are close to those of shown in Ref. [83]; see Table III for the values of Ref. [83].

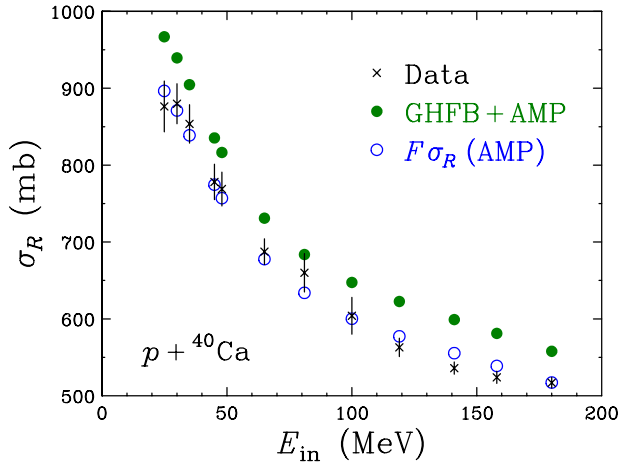


FIG. 7. E_{in} dependence of reaction cross sections σ_R for $p+^{40}\text{Ca}$ scattering. Closed circles denote results of the original (D1S-GHFB+AMP) densities and the scaled ones, Open circles correspond to $F\sigma_R(\text{AMP})$. The data (crosses) are taken from Refs. [50–52].

5. ^{12}C

Figure 8 shows σ_R as a function of E_{in} for $p+^{12}\text{C}$ scattering. The results $\sigma_R(\text{AMP})$ of D1S-GHFB+AMP overshoot data $\sigma_R(\text{exp})$ [51, 52, 72].

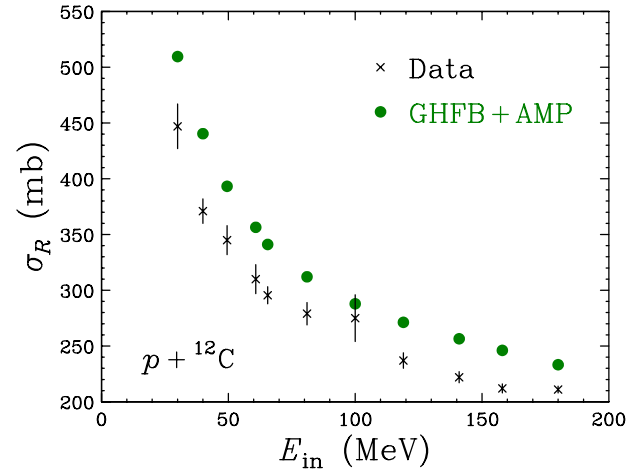


FIG. 8. E_{in} dependence of reaction cross sections σ_R for $p+^{12}\text{C}$ scattering. Closed circles denote results $F\sigma_R(\text{AMP})$. The data (crosses) are taken from Refs. [51, 52, 72].

Figure 9 shows $\sigma_R(\text{GSI})$ based on $r_m(\text{GSI})$ and $r_p(\text{exp}) = 2.327$ fm of electron scattering for $p+^{12}\text{C}$ scattering. The results $\sigma_R(\text{GSI})$ are near the upper bound of $\sigma_R(\text{exp})$ [51, 52, 72]. The $F\sigma_R(\text{GSI})$ (open circles) are near the central values of $\sigma_R(\text{exp})$.

The result of ESP-F is $r_m(\text{exp}) = 2.340 \pm 0.009$ fm. Using the $r_m(\text{exp})$ and $r_p(\text{exp}) = 2.327$ fm, we can obtain $r_{\text{skin}}(\text{exp}) = 0.026 \pm 0.009$ fm and $r_n(\text{exp}) = 2.354 \pm 0.009$ fm.

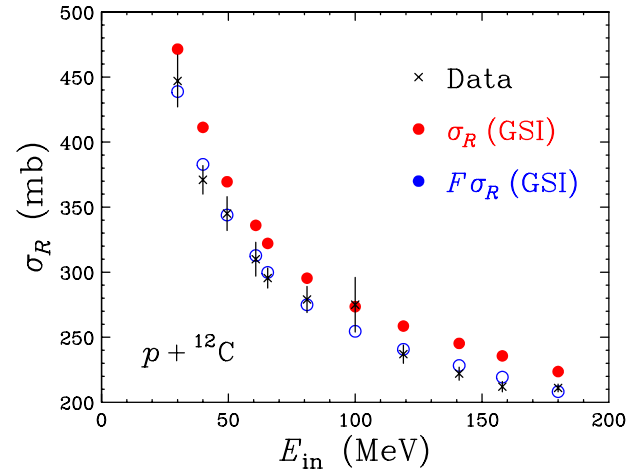


FIG. 9. E_{in} dependence of reaction cross sections σ_R for $p+^{12}\text{C}$ scattering. Closed circles denote results $\sigma_R(\text{GSI})$, while open circles correspond to $F\sigma_R(\text{GSI})$. The data (crosses) are taken from Refs. [51, 52, 72].

Tanihata *et al.* determined r_m from interaction cross sections for He, Li, Be, B isotopes [84]. In Ref. [86], the experimental values on r_m are accumulated from ^4He to ^{32}Mg . Our result $r_m(\text{exp}) = 2.340 \pm 0.009$ fm is slightly smaller to $r_m(\text{GSI}) = 2.35(2)$ fm. As for neutron radius, this is the

case, because $r_n(\text{exp}) = 2.354 \pm 0.009$ fm and $r_n(\text{GSI}) = 2.37(2)$ fm.

IV. SUMMARY

In this paper, we consider the ^{208}Pb , ^{58}Ni , $^{40,48}\text{Ca}$, ^{12}C , as stable nuclei and determine $r_{\text{skin}}(\sigma_R)$, $r_m(\sigma_R)$, $r_n(\sigma_R)$ from measured σ_R . Our results on $r_{\text{skin}}(\sigma_R)$, $r_m(\sigma_R)$, $r_n(\sigma_R)$, are summarized in Table V. Comparing Table V with Table III, we find that our results are close to the reference values.

TABLE V. Our results for r_m , r_n , r_{skin} . The radii are shown in units of fm.

	$r_m(\sigma_R)$	$r_n(\sigma_R)$	$r_{\text{skin}}(\sigma_R)$
^{208}Pb	5.627 ± 0.020	5.743 ± 0.020	0.299 ± 0.020
^{58}Ni	3.711 ± 0.010	3.740 ± 0.010	0.055 ± 0.010
^{48}Ca	3.445 ± 0.022	3.488 ± 0.022	0.103 ± 0.022
^{40}Ca	3.372 ± 0.011	3.367 ± 0.011	-0.011 ± 0.011
^{12}C	2.340 ± 0.009	2.354 ± 0.009	0.026 ± 0.009

We show mass-number (A) dependence of stable nuclei in Figs. 10, 11, 12. Figure 10 shows skin values as a function of $S_p - S_n$, where S_p (S_n) is the proton (neutron) separation energy. The skin values $r_{\text{skin}}(\sigma_R)$ determined from measured σ_R for ^{208}Pb , ^{58}Ni , $^{40,48}\text{Ca}$ are compared with the data of PREX2 [5], $^{116,118,120,122,124}\text{Sn}$ [87, 88], ^{48}Ca [45]. Our results are consistent with the previous experimental skin values.

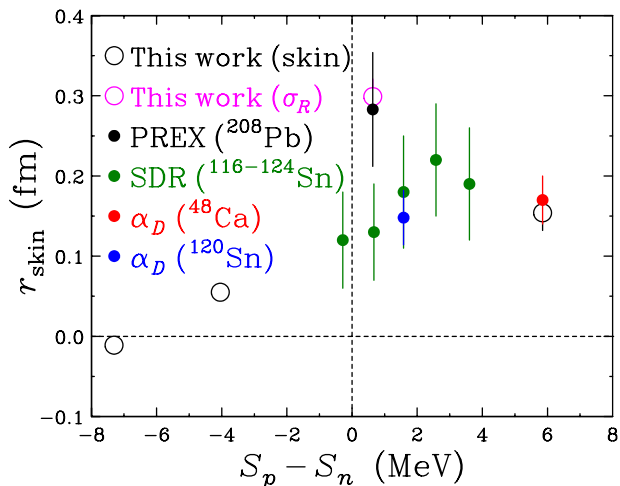


FIG. 10. Skin values as a function of $S_p - S_n$. The skin values determined from measured σ_R are shown with “This work (skin)” for ^{208}Pb and with “This work (σ_R)” for ^{58}Ni , $^{40,48}\text{Ca}$. The symbol “ α_D ” means the results of the $E1$ polarizability experiment ($E1pE$) for ^{120}Sn [88] and ^{48}Ca [45]. The symbol “PREX” stands for the result deduced from $r_{\text{skin}}^{208}(\text{PREX2}) = 0.283 \pm 0.071$ fm. Open circles stand for the results of this work. The symbol “SDR” shows the results [87] of the measurement based on the isovector spin-dipole resonances (SDR) in Sn isotopes. The data (closed circles with error bar) are taken from Refs. [5, 45, 87, 88].

Figure 11 shows matter radii r_m as a function of $A^{1/3}$. For ^{208}Pb , $^{116,118,120,122,124}\text{Sn}$, ^{48}Ca , the r_m are derived from the corresponding skin values [5, 45, 87, 88] and the corresponding r_p of electron scattering. For ^{12}C , $^{40,48}\text{Ca}$, ^{58}Ni , ^{208}Pb , our results are added. Our results are consistent with the previous works.

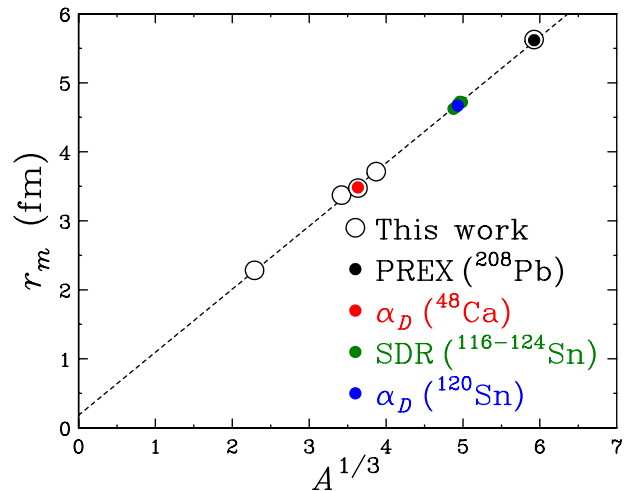


FIG. 11. Matter radii r_m as a function of mass number $A^{1/3}$. The symbol “ α_D ” means the results of the $E1$ polarizability experiment ($E1pE$) for ^{120}Sn [88] and ^{48}Ca [45]. The symbol “PREX” stands for the result deduced from $r_{\text{skin}}^{208}(\text{PREX2}) = 0.283 \pm 0.071$ fm. The symbol “SDR” shows the results [87] of the measurement based on the isovector spin-dipole resonances (SDR) in the Sb isotopes. Open circles stand for the results of this work. The dashed line is a guide for the eyes. The data (closed circles with error bar) are taken from Refs. [5, 45, 87, 88].

Figure 12 shows neutron radii r_n as a function of mass number $A^{1/3}$. For ^{208}Pb , $^{116,118,120,122,124}\text{Sn}$, ^{48}Ca , the r_n are derived from the corresponding skin values [5, 45, 87, 88] and the corresponding r_p of electron scattering. For ^{12}C , $^{40,48}\text{Ca}$, ^{58}Ni , ^{208}Pb , our results are added. Our results are consistent with the previous works.

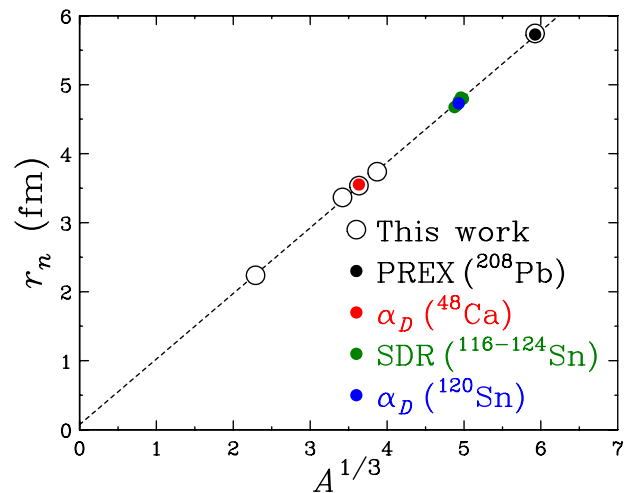


FIG. 12. Neutron radii r_n as a function of mass number $A^{1/3}$. The symbol “ α_D ” means the results of the $E1$ polarizability experiment ($E1pE$) for ^{120}Sn [88] and ^{48}Ca [45]. The symbol “PREX” stands for the result deduced from r_{skin}^{208} (PREX2) = 0.283 ± 0.071 fm. The symbol “SDR” shows the results [87] of the measurement based on the isovector spin-dipole resonances (SDR) in the Sb isotopes. Open circles stand for the results of this work. The dashed line is a guide for the eyes. The data (closed circles with error bar) are taken from Refs. [5, 45, 87, 88].

ACKNOWLEDGMENTS

We would like to thank Dr. Toyokawa for providing his code and Prof. M. Nakano for useful information.

-
- [1] X. Roca-Maza, M. Centelles, X. Vinas, and M. Warda, *Phys. Rev. Lett.* **106**, 252501 (2011), arXiv:1103.1762 [nucl-th].
- [2] C. J. Horowitz, S. J. Pollock, P. A. Souder, and R. Michaels, *Phys. Rev. C* **63**, 025501 (2001).
- [3] S. Abrahamyan, Z. Ahmed, H. Albatineh, K. Aniol, D. S. Armstrong, W. Armstrong, T. Averett, B. Babineau, A. Barbieri, V. Bellini, et al. (PREX Collaboration), *Phys. Rev. Lett.* **108**, 112502 (2012).
- [4] C. J. Horowitz, Z. Ahmed, C.-M. Jen, A. Rakhman, P. A. Souder, M. M. Dalton, N. Liyanage, K. D. Paschke, K. Saenboonruang, R. Silwal, G. B. Franklin, M. Friend, B. Quinn, K. S. Kumar, D. McNulty, L. Mercado, S. Riordan, J. Wexler, R. W. Michaels, and G. M. Urciuoli, *Phys. Rev. C* **85**, 032501 (2012).
- [5] D. Adhikari et al. (PREX), *Phys. Rev. Lett.* **126**, 172502 (2021), arXiv:2102.10767 [nucl-ex].
- [6] A. Trzcińska, J. Jastrzębski, P. Lubiński, F. J. Hartmann, R. Schmidt, T. von Egidy, and B. Klos, *Phys. Rev. Lett.* **87**, 082501 (2001).
- [7] J. Zenihiro, H. Sakaguchi, T. Murakami, M. Yosoi, Y. Yasuda, S. Terashima, Y. Iwao, et al., *Phys. Rev. C* **82**, 044611 (2010).
- [8] A. Tamii, I. Poltoratska, P. von Neumann-Cosel, Y. Fujita, T. Adachi, C. A. Bertulani, J. Carter, et al., *Phys. Rev. Lett.* **107**, 062502 (2011).
- [9] C. M. Tarbert, D. P. Watts, D. I. Glazier, P. Aguar, J. Ahrens, J. R. M. Annand, H. J. Arends, R. Beck, V. Bekrenev, B. Boillat, et al. (Crystal Ball at MAMI and A2 Collaboration), *Phys. Rev. Lett.* **112**, 242502 (2014).
- [10] M. C. Atkinson, M. H. Mahzoon, M. A. Keim, B. A. Bordelon, C. D. Pruitt, R. J. Charity, and W. H. Dickhoff, *Phys. Rev. C* **101**, 044303 (2020).
- [11] D. Adhikari et al. (CREX), *Phys. Rev. Lett.* **129**, 042501 (2022), arXiv:2205.11593 [nucl-ex].
- [12] S. J. Novario, G. Hagen, G. R. Jansen, and T. Papenbrock, *Phys. Rev. C* **102**, 051303 (2020).
- [13] H. Shen, F. Ji, J. Hu, and K. Sumiyoshi, *Astrophys. J.* **891**, 148 (2020).
- [14] C. Horowitz, *Ann. Phys. (Amsterdam)* **411**, 167992 (2019).
- [15] Wei, Jin-Biao, Lu, Jia-Jing, Burgio, G. F., Li, Zeng-Hua, and Schulze, H.-J., *Eur. Phys. J. A* **56**, 63 (2020).
- [16] M. Thiel, C. Sienti, J. Piekarewicz, C. J. Horowitz, and M. Vanderhaeghen, *J. Phys. G: Nucl. Part. Phys.* **46**, 093003 (2019).
- [17] B. T. Reed, F. J. Fattoyev, C. J. Horowitz, and J. Piekarewicz, *Phys. Rev. Lett.* **126**, 172503 (2021), arXiv:2101.03193 [nucl-th].

- [18] S. Tagami, T. Wakasa, M. Takechi, J. Matsui, and M. Yahiro, *Results in Physics* **33**, 105155 (2022).
- [19] A. Akmal, V. R. Pandharipande, and D. G. Ravenhall, *Phys. Rev. C* **58**, 1804 (1998), arXiv:nucl-th/9804027.
- [20] C. Ishizuka, T. Suda, H. Suzuki, A. Ohnishi, K. Sumiyoshi, and H. Toki, *Publ. Astron. Soc. Jap.* **67**, 13 (2015), arXiv:1408.6230 [nucl-th].
- [21] C. Gonzalez-Boquera, M. Centelles, X. Viñas, and L. M. Robledo, *Phys. Lett. B* **779**, 195 (2018), arXiv:1712.06735 [nucl-th].
- [22] M. Farine, D. Von-Eiff, P. Schuck, J. F. Berger, J. Dechargé, and M. Girod, **25**, 863 (1999).
- [23] C. Gonzalez-Boquera, M. Centelles, X. Viñas, and A. Rios, *Phys. Rev. C* **96**, 065806 (2017), arXiv:1706.02736 [nucl-th].
- [24] M. Oertel, M. Hempel, T. Klähn, and S. Typel, *Rev. Mod. Phys.* **89**, 015007 (2017), arXiv:1610.03361 [astro-ph.HE].
- [25] J. Piekarewicz, *Phys. Rev. C* **76**, 064310 (2007), arXiv:0709.2699 [nucl-th].
- [26] Y. Lim, K. Kwak, C. H. Hyun, and C.-H. Lee, *Phys. Rev. C* **89**, 055804 (2014), arXiv:1312.2640 [nucl-th].
- [27] R. Sellahewa and A. Rios, *Phys. Rev. C* **90**, 054327 (2014), arXiv:1407.8138 [nucl-th].
- [28] T. Inakura and H. Nakada, *Phys. Rev. C* **92**, 064302 (2015), arXiv:1509.02982 [nucl-th].
- [29] F. J. Fattoyev and J. Piekarewicz, *Phys. Rev. Lett.* **111**, 162501 (2013), arXiv:1306.6034 [nucl-th].
- [30] A. W. Steiner, M. Prakash, J. M. Lattimer, and P. J. Ellis, *Phys. Rept.* **411**, 325 (2005), arXiv:nucl-th/0410066.
- [31] M. Centelles, X. Roca-Maza, X. Vinas, and M. Warda, *Phys. Rev. C* **82**, 054314 (2010), arXiv:1010.5396 [nucl-th].
- [32] M. Dutra, O. Lourenco, J. S. Sa Martins, A. Delfino, J. R. Stone, and P. D. Stevenson, *Phys. Rev. C* **85**, 035201 (2012), arXiv:1202.3902 [nucl-th].
- [33] B. A. Brown and A. Schwenk, *Phys. Rev. C* **89**, 011307 (2014), [Erratum: *Phys.Rev.C* 91, 049902 (2015)], arXiv:1311.3957 [nucl-th].
- [34] B. A. Brown, *Phys. Rev. Lett.* **85**, 5296 (2000).
- [35] P. G. Reinhard, A. S. Umar, P. D. Stevenson, J. Piekarewicz, V. E. Oberacker, and J. A. Maruhn, *Phys. Rev. C* **93**, 044618 (2016), arXiv:1603.01319 [nucl-th].
- [36] C. Y. Tsang, B. A. Brown, F. J. Fattoyev, W. G. Lynch, and M. B. Tsang, *Phys. Rev. C* **100**, 062801 (2019), arXiv:1908.11842 [nucl-th].
- [37] C. Ducoin, J. Margueron, and C. Providencia, *EPL* **91**, 32001 (2010), arXiv:1004.5197 [nucl-th].
- [38] M. Fortin, C. Providencia, A. R. Raduta, F. Gulminelli, J. L. Zdunik, P. Haensel, and M. Bejger, *Phys. Rev. C* **94**, 035804 (2016), arXiv:1604.01944 [astro-ph.SR].
- [39] L.-W. Chen, C. M. Ko, B.-A. Li, and J. Xu, *Phys. Rev. C* **82**, 024321 (2010), arXiv:1004.4672 [nucl-th].
- [40] P. W. Zhao and S. Gandolfi, *Phys. Rev. C* **94**, 041302 (2016), arXiv:1604.01490 [nucl-th].
- [41] Z. Zhang, Y. Lim, J. W. Holt, and C. M. Ko, *Phys. Lett. B* **777**, 73 (2018), arXiv:1703.00866 [nucl-th].
- [42] Y. Wang, C. Guo, Q. Li, H. Zhang, Y. Leifels, and W. Trautmann, *Phys. Rev. C* **89**, 044603 (2014), arXiv:1403.7041 [nucl-th].
- [43] O. Lourenço, M. Bhuyan, C. H. Lenzi, M. Dutra, C. Gonzalez-Boquera, M. Centelles, and X. Viñas, *Phys. Lett. B* **803**, 135306 (2020), arXiv:2002.06242 [nucl-th].
- [44] A. Tamii et al., *Phys. Rev. Lett.* **107**, 062502 (2011), arXiv:1104.5431 [nucl-ex].
- [45] J. Birkhan et al., *Phys. Rev. Lett.* **118**, 252501 (2017), arXiv:1611.07072 [nucl-ex].
- [46] S. Tagami, T. Wakasa, J. Matsui, M. Yahiro, and M. Takechi, *Phys. Rev. C* **104**, 024606 (2021), arXiv:2010.02450 [nucl-th].
- [47] M. Matsuzaki, S. Tagami, and M. Yahiro, *Phys. Rev. C* **104**, 054613 (2021), arXiv:2107.06441 [nucl-th].
- [48] M. Toyokawa, M. Yahiro, T. Matsumoto, and M. Kohno, *PTEP* **2018**, 023D03 (2018), arXiv:1712.07033 [nucl-th].
- [49] S. Tagami, M. Tanaka, M. Takechi, M. Fukuda, and M. Yahiro, *Phys. Rev. C* **101**, 014620 (2020).
- [50] R. F. Carlson, A. J. Cox, J. R. Nimmo, N. E. Davison, S. A. Elbahr, J. L. Horton, A. Houdayer, A. M. Sourkes, W. T. H. Van Oers, and D. J. Margaziotis, *Phys. Rev. C* **12**, 1167 (1975).
- [51] A. Ingemarsson et al., *Nucl. Phys. A* **653**, 341 (1999).
- [52] A. Auce et al., *Phys. Rev. C* **71**, 064606 (2005).
- [53] A. B. Jones and B. A. Brown, *Phys. Rev. C* **90**, 067304 (2014).
- [54] S. Kox, A. Gamp, C. Perrin, J. Arvieux, R. Bertholet, J. F. Bruandet, M. Buenerd, Y. El Masri, N. Longequeue, and F. Merchez, *Phys. Lett. B* **159**, 15 (1985).
- [55] F. Brieva and J. Rook, *Nucl. Phys. A* **291**, 299 (1977); *Nucl. Phys. A* **291**, 317 (1977); *Nucl. Phys. A* **297**, 206 (1978).
- [56] G. Satchler and W. Love, *Physics Reports* **55**, 183 (1979); G. R. Satchler, *Direct Nuclear Reactions* (Oxford University Press, 1983).
- [57] N. Yamaguchi, S. Nagata, and T. Matsuda, *Prog. Theor. Phys.* **70**, 459 (1983); S. Nagata, M. Kamimura, and N. Yamaguchi, *Prog. Theor. Phys.* **73**, 512 (1985); N. Yamaguchi, S. Nagata, and J. Michiyama, *Prog. Theor. Phys.* **76**, 1289 (1986).
- [58] K. Amos, P. J. Dortmans, H. V. von Geramb, S. Karataglidis, and J. Raynall, “Nucleon-nucleus scattering: A microscopic nonrelativistic approach,” in *Advances in Nuclear Physics*, edited by J. W. Negele and E. Vogt (Springer US, Boston, MA, 2000) pp. 276–536.
- [59] T. Furumoto, Y. Sakuragi, and Y. Yamamoto, *Phys. Rev. C* **78**, 044610 (2008); *Phys. Rev. C* **79**, 011601 (2009); *Phys. Rev. C* **80**, 044614 (2009).
- [60] K. Egashira, K. Minomo, M. Toyokawa, T. Matsumoto, and M. Yahiro, *Phys. Rev. C* **89**, 064611 (2014).
- [61] M. Toyokawa, K. Minomo, M. Kohno, and M. Yahiro, *J. Phys. G: Nucl. Part. Phys.* **42**, 025104 (2014); *J. Phys. G: Nucl. Part. Phys.* **44**, 079502 (2017).
- [62] M. Toyokawa, M. Yahiro, T. Matsumoto, K. Minomo, K. Ogata, and M. Kohno, *Phys. Rev. C* **92**, 024618 (2015); *Phys. Rev. C* **96**, 059905(E) (2017).
- [63] M. Toyokawa, M. Yahiro, T. Matsumoto, and M. Kohno, *Prog. Theor. Exp. Phys.* **2018**, 023D03 (2018).
- [64] K. Minomo, T. Sumi, M. Kimura, K. Ogata, Y. R. Shimizu, and M. Yahiro, *Phys. Rev. Lett.* **108**, 052503 (2012).
- [65] M. Takechi et al., *Phys. Lett. B* **707**, 357 (2012).
- [66] T. Sumi, K. Minomo, S. Tagami, M. Kimura, T. Matsumoto, K. Ogata, Y. R. Shimizu, and M. Yahiro, *Phys. Rev. C* **85**, 064613 (2012).
- [67] S. Watanabe, K. Minomo, M. Shimada, S. Tagami, M. Kimura, M. Takechi, M. Fukuda, D. Nishimura, T. Suzuki, T. Matsumoto, et al., *Phys. Rev. C* **89**, 044610 (2014).
- [68] T. Eliyakut-Roshko, R. H. McCamis, W. T. H. van Oers, R. F. Carlson, and A. J. Cox, *Phys. Rev. C* **51**, 1295 (1995).
- [69] J. F. Dicello, G. J. Igo, and M. L. Roush, *Phys. Rev.* **157**, 1001 (1967).
- [70] P. J. Bulman and J. A. R. Griffith, *Nucl. Phys. A* **111**, 315 (1968).
- [71] R. F. Carlson, A. J. Cox, N. E. Davison, T. Eliyakut-Roshko, R. H. McCamis, and W. T. H. v. Oers, *Phys. Rev. C* **49**, 3090 (1994).
- [72] J. J. H. Menet, E. E. Gross, J. J. Malanify, and A. Zucker, *Phys. Rev. C* **4**, 1114 (1971).

- [73] T. Wakasa, S. Tagami, J. Matsui, M. Yahiro, and M. Takechi, *Results in Physics* **29**, 104749 (2021).
- [74] M. Kohno, *Phys. Rev. C* **88**, 064005 (2013); *Phys. Rev. C* **96**, 059903(E) (2017).
- [75] H. V. von Geramb, K. Amos, L. Berge, S. Bräutigam, H. Kohlhoff, and A. Ingemarsson, *Phys. Rev. C* **44**, 73 (1991).
- [76] P. J. Dortmans and K. Amos, *Phys. Rev. C* **49**, 1309 (1994).
- [77] J. Fujita and H. Miyazawa, *Prog. Theor. Phys.* **17**, 360 (1957); *Prog. Theor. Phys.* **17**, 366 (1957).
- [78] M. Toyokawa, K. Minomo, M. Kohno, and M. Yahiro, *J. Phys. G* **42**, 025104 (2015), [Erratum: *J. Phys. G* **44**, 079502 (2017)], arXiv:1404.6895 [nucl-th].
- [79] S. Tagami, M. Tanaka, M. Takechi, M. Fukuda, and M. Yahiro, *Phys. Rev. C* **101**, 014620 (2020), arXiv:1911.05417 [nucl-th].
- [80] K. Minomo, K. Ogata, M. Kohno, Y. R. Shimizu, and M. Yahiro, *J. Phys. G* **37**, 085011 (2010), arXiv:0911.1184 [nucl-th].
- [81] T. Sumi, K. Minomo, S. Tagami, M. Kimura, T. Matsumoto, K. Ogata, Y. R. Shimizu, and M. Yahiro, *Phys. Rev. C* **85**, 064613 (2012), arXiv:1201.2497 [nucl-th].
- [82] I. Angeli and K. P. Marinova, *Atom. Data Nucl. Data Tabl.* **99**, 69 (2013).
- [83] J. Zenihiro *et al.*, (2018), arXiv:1810.11796 [nucl-ex].
- [84] I. Tanihata, T. Kobayashi, O. Yamakawa, S. Shimoura, K. Ekuni, K. Sugimoto, N. Takahashi, T. Shimoda, and H. Sato, *Phys. Lett. B* **206**, 592 (1988).
- [85] J. C. Zamora *et al.*, *Phys. Rev. C* **96**, 034617 (2017).
- [86] A. Ozawa, T. Suzuki, and I. Tanihata, *Nucl. Phys. A* **693**, 32 (2001).
- [87] A. Krasznahorkay *et al.*, *Phys. Rev. Lett.* **82**, 3216 (1999).
- [88] T. Hashimoto *et al.*, *Phys. Rev. C* **92**, 031305 (2015), arXiv:1503.08321 [nucl-ex].